# A Two-Level Hysteresis-Based Sliding Mode Control for Three-Level Single-Phase Inverters

Víctor Repecho, Abel Borràs, and Domingo Biel

***Abstract*—In this article, we present a single-phase inverter controlled by a three-level sliding mode control. A simple first order sliding mode is designed to regulate the output voltage and it is implemented through a symmetrical two-level hysteresis band comparator. The hysteresis band of the comparator is dynamically adjusted to bound the switching frequency of the inverter. As a result, the desired voltage tracking is achieved and no average error is induced at the output. The article includes numerical simulation and experimental results carried out in a 1.2 kW prototype that confirm the good performance of the designed control in terms of tracking error and harmonic distortion of the output voltage. The proposal has been tested with input voltage variations, transients of resistive loads and with a nonlinear load showing the expected robustness.**

***Index Terms*—Sliding mode control (SMC), three-level inverter, two-level hysteresis band comparators.**

## I. Introduction

THE benefits of the sliding mode control (SMC), such as robustness, insensitivity to parametric variations and good transient response have been widely reported in the control literature over the years [1]. One of the limitations for the application of its original version, known as first order sliding mode control (FOSMC), is the fact that the control laws are based on discontinuous control signals. The discontinuity in the control signal provides the aforementioned benefits, but also constitutes its main drawback when it has to be implemented. Furthermore, in the case when the discontinuous controls can be implemented, the resulting signal commutates at variable switching frequency, depending on the system state, which is often considered a disadvantage. These characteristics restrict its application in systems with continuous control signals. However, this feature does not represent a limitation on power electronics [2], where the control signals are inherently discontinuous, since they are driving solid state switches. Among others, several approaches addressing the issue of variable switching frequency can be mentioned here, such as the application of efficient algorithms to set the switching frequency but with complex calculations and fast processing requirements [3], [4], [5], [6], the use of continuous control signals extracted from the switching surface acting as duty cycle of a pulsewidth modulator (PWM) [7], [8], [9], [10], [11], [12], to regulate the switching frequency by means of an external controller [13], [14], [15], or to dynamically adjust the hysteresis band to set the average switching frequency by minimizing the variation around the desired value [16].

Among the different power stages, the full-bridge converter, and specifically the voltage source inverter (VSI), can be pointed out as one of the most widely used. This topology is used in many applications, such as machine drives, grid-connected inverters, and uninterruptible power supply systems. The main control specifications for this converter can be focused on power quality [total harmonic distortion (THD) and power factor control] and voltage regulation, and when linear controllers are used, such as resonant proportional (PR) controllers, for example, see [20], [21], and [22], they are well met. SMC applied to this problem has also been researched, mainly to enhance the robustness and transient response of the inverter when the load or input voltage changes. As an example, a comparative study showing the improvements of a FOSMC over a PR control can be found in [15].

Unlike elementary topologies, the full-bridge structure can generate a third voltage level at its differential output, a null level, which may or may not be used. This issue is known as two-level (bipolar) and three-level (unipolar) modulation strategies [23]. The main benefit of three-level modulation, compared to the two-level mode, is the lower ripple of the state variables for the same switching frequency, which reduces the power losses. In PWM switched-mode power converters, both strategies can be easily implemented, see Fig. 1(a) and (b). Two-level modulation is obtained with a single comparator and a carrier signal fixing the switching frequency and three-level mode is generated by adding another comparator and inverting the control signal.

Concerning the SMC, the FOSMC is based on defining a switching surface, $\sigma := 0$, where the switching function $\sigma$ is enforced to slide. A discontinuous control, $u$, based on the sign of $\sigma$, is designed to impose $\sigma = 0$. Once the switching function slides over $\sigma = 0$, the desired dynamics are obtained. For the output voltage regulation of a VSI, $\sigma$ is an scalar and the control only takes two values, one when $\sigma > 0$ and another when $\sigma < 0$. Therefore, the application of a FOSMC in a VSI directly leads to a two-level implementation. Fig. 1(c) shows a two-level implementation using a hysteresis comparator instead

Received 4 March 2025; revised 23 May 2025; accepted 10 June 2025. Date of publication 24 June 2025; date of current version 5 August 2025. This work was supported in part by the Government of Spain through the *Agencia Estatal de Investigación* Project under Grant PID2021-122821NB-I00 and in part by the *Generalitat de Catalunya* through the Project 2021 under Grant SGR 00376. Recommended for publication by Associate Editor J. He. *(Corresponding author: Víctor Repecho.)*

The authors are with the Institute of Industrial and Control Engineering IOC, Universitat Politècnica de Catalunya, 08028 Barcelona, Spain (e-mail: victor.repecho.del@upc.edu; domingo.biel@upc.edu).

Color versions of one or more figures in this article are available at https://doi.org/10.1109/TPEL.2025.3582019.

Digital Object Identifier 10.1109/TPEL.2025.3582019

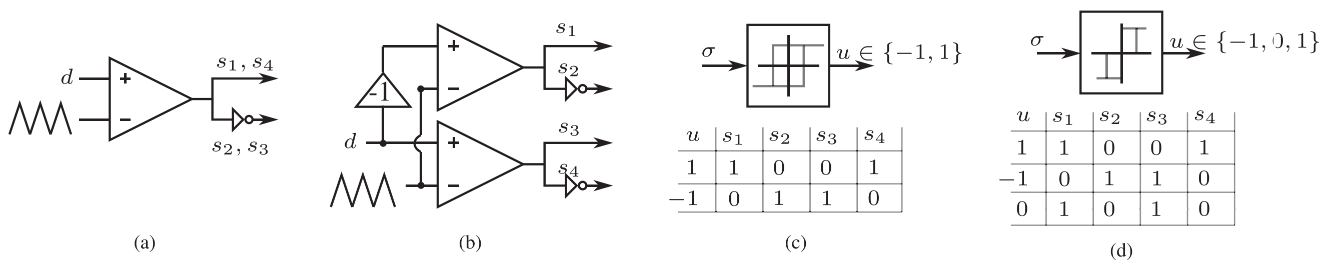


(c)

| $u$ | $s_1$ | $s_2$ | $s_3$ | $s_4$ |
|---|---|---|---|---|
| 1 | 1 | 0 | 0 | 1 |
| −1 | 0 | 1 | 1 | 0 |

(d)

| $u$ | $s_1$ | $s_2$ | $s_3$ | $s_4$ |
|---|---|---|---|---|
| 1 | 1 | 0 | 0 | 1 |
| −1 | 0 | 1 | 1 | 0 |
| 0 | 1 | 0 | 1 | 0 |

Fig. 1. (a) Two-level PWM implementation. (b) Three-level PWM implementation. (c) Two-level FOSMC implementation. (d) Three-level FOSM implementation proposed in [17], [18], and [19]. $s_i$, with $i \in \{1, 2, 3, 4\}$, represents the state of the power switch of the inverter full-bridge, see Fig. 2. $s_i = 0$ means switch open and $s_i = 1$ stands for switch closed.

of the sign function, where the hysteresis band bounds the switching frequency. As the comparator has only two output states, it is straightforward to map the FOSMC values to the inverter power switches by applying the table shown in the same figure. This approach is proposed in some references, such as [8], [12], [15], [24], [25], or [26], for instance. Nevertheless, while the implementation of the two-level FOSMC is straightforward and simple, attempting a three-level implementation of the control signal is not, and this involves a problem to overcome. Thus, the problem is to find a procedure that assigns each of the three levels of the control signal according to the state of the FOSMC switching function, so that the resulting behavior becomes similar to the ideal sliding dynamics while guaranteeing its performance and preserving an admissible tracking error. To the best of the authors' knowledge, there are very few references, discussed below, that have studied this issue. Namely, the approach in [8] where an implementation using a sign function approximation based on a saturated linear action obtaining a boundary layer sliding mode was presented. The proposal allows the use of PWM to perform the three-level switching but the properties of the sliding mode are no longer guaranteed. Indeed, the proposal uses the three-level PWM implementation shown in Fig. 1(b). The authrs in [17], [18], and [19] proposed a controller based on a double band hysteresis comparator, see Fig. 1(d). The results of the cited research studies show good overall performance and, as expected, a reduction in current ripple is achieved by the three-level implementation. However, as the implementation used a double band hysteresis comparator, the value of the switching function when averaging over half of the reference period took a nonzero value, thus inducing an error in the output voltage. This problem is tackled by using proportional–integral, see for instance [19], or PR controllers, as presented in [27], which add additional dynamics to that provided by the SMC. Finally, it is worth mentioning here the work [28] where this concept is extended to the hysteretic staircase comparator, which is applied to a full-bridge multilevel converter.

The main contribution of this work is the development of a methodology for implementing a FOSMC with three-level operation having the following characteristics:

1) The proposed control law automatically adapts the proper combination of power switches that guarantees the sliding regime and reduce the ripple of the converter variables.
2) The switching function, under sliding motion and at steady state, is always confined within a single two-level hysteresis comparator with symmetrical band centered at zero, and, as a consequence, there is no averaged error induced at the voltage output.
3) The hysteresis band is adapted to operate within a small bandwidth around a certain switching frequency.

The rest of this article is organized as follows. Section II states the structure of the single-phase inverter and its dynamical model. In Section III, the design, stability, and robustness of the SMC and the proposed control law for three-level operation are detailed. The implementation of the three-level control and the switching function expected behavior in a realistic case are presented in Section IV. The design of the variable hysteresis band to bound the switching frequency and numerical simulation results confirming the expected performance are shown in Section IV-C. Subsequently, Section V contains the implementation details where the experimental setup and the controller discretization are detailed. Section VI shows the corresponding results obtained on a 1.2 kW inverter. For comparison purposes, all the experimental results are carried out in both two- and three-level operation and with fixed and variable hysteresis band in Section VII. Finally, Section VIII concludes this article.

## II. VSI Topology

The well-known topology of a full-bridge VSI is shown in Fig. 2, where $\frac{E}{2}$ represent the semi-bus voltage with respect the reference point, $L$ and $C$ are the reactive components, and $i_o$ is the output current delivered to the load. It is assumed that $i_o$ is a function of the output voltage, i.e., $i_o = f(v_c)$, ($f(v_c) = \frac{v_c}{R}$ for a resistive load). The dynamics of the converter can be modeled by the equations

$$\frac{di_L}{dt} = \frac{1}{L}\left(v_a - v_b - v_c\right) \tag{1a}$$

$$\frac{dv_c}{dt} = \frac{1}{C}\left(i_L - i_o\right). \tag{1b}$$

From the discrete operation of the switches, one can see that the voltages at the center point of each leg $(v_a, v_b)$ can only take two discrete values: $\frac{E}{2}$ when $s_1$ or $s_3$ are closed or $-\frac{E}{2}$ when

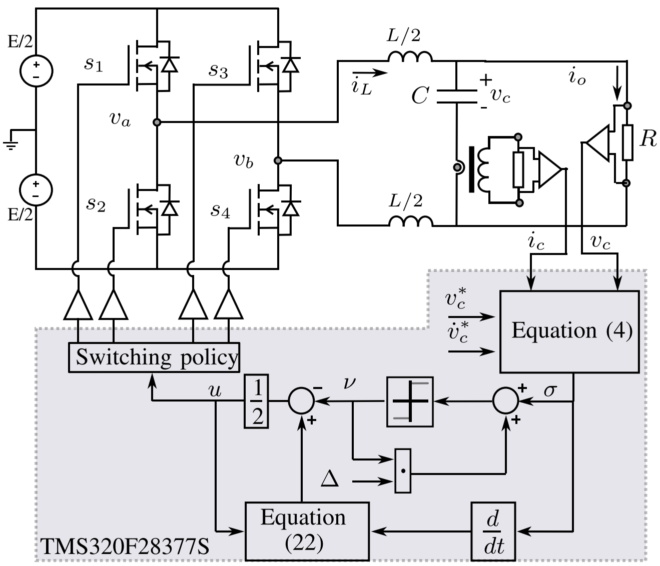


Fig. 2. Scheme of the VSI with the proposed controller.

the closed ones are $s_2$ or $s_4$. Generally speaking, if the control algorithm allows that $s_1$ and $s_3$ (or $s_2$ and $s_4$) are closed at the same time the system works with three-level modulation and the voltage $v_a - v_b$ is unipolar taken values 0 and $E$ or $-E$ and 0. Otherwise, the converter operates in two-level modulation, $v_a - v_b$ is bipolar and can only takes $E$ or $-E$ values. Therefore, when all the switches combinations are allowed, the control signal is defined as $u \in \{-1, 0, 1\}$, and with the previous definitions the state space equation can be rewritten as

$$\frac{di_L}{dt} = \frac{1}{L}\left(E\,u - v_c\right) \tag{2a}$$

$$\frac{dv_c}{dt} = \frac{1}{C}\left(i_L - i_o\right). \tag{2b}$$

## III. SMC of a VSI

### A. Switching Function Definition

The control objective of the converter is to track a time-varying reference voltage at the output of the *LC* filter. The desired output voltage is

$$v_c^* = A \sin \omega t. \tag{3}$$

According to the relative degree from the control input to the output voltage, the following switching function is proposed:

$$\sigma =: e_v + \alpha\, \dot{e}_v \tag{4}$$

where $e_v = v_c - v_c^*$.

Applying time derivative to (4), and replacing (2a), the sliding mode equation is found as

$$\dot{\sigma} = \dot{v}_c - \frac{\alpha}{C}\frac{di_o}{dt} + \frac{\alpha}{LC}\left(Eu - v_c\right) - \dot{v}_c^* - \alpha \ddot{v}_c^* \tag{5}$$

and the equivalent control [1] can be found assuming that $\dot{\sigma} = 0$

$$u_{eq} = \frac{v_c}{E} + \frac{LC}{\alpha E}\left[\frac{\alpha}{C}\frac{di_o}{dt} - \dot{v}_c + \dot{v}_c^* + \alpha \ddot{v}_c^*\right]. \tag{6}$$

Finally, merging (5) and (6) yields

$$\dot{\sigma} = \frac{E\alpha}{LC}\left(u - u_{\text{eq}}\right). \tag{7}$$

Sliding mode is enforced when $\sigma\dot{\sigma} < 0$. Therefore, sliding regime requires the fulfilment of

$$\sigma \frac{E\alpha}{LC}\left(u - u_{\text{eq}}\right) < 0. \tag{8}$$

### B. Proposed Control Law for Three-Level Operation

When working with two-level modulation, the control signal only takes two possible values, i.e., $u \in \{-1, 1\}$, and the control assignment to fulfil (8) is just straightforward

$$\sigma \frac{E\alpha}{LC}\left(u - u_{\text{eq}}\right) < 0 \Rightarrow u = -\text{sign}(\sigma). \tag{9}$$

Therefore, in the standard FOSMC [1] the possibility to apply the "0" control state of $u$ is directly omitted. This simplifies the control implementation and the sign function is carried out by means of a hysteresis comparator, but produces higher current ripples and losses in the system when compared to three-level modulation operating at same switching frequency. In order to reduce the losses, a three-level control law is proposed as

$$u = \frac{1}{2}\left[\text{sign}(u_{eq}) - \text{sign}(\sigma)\right]. \tag{10}$$

Notice that the function $\text{sign}(u_{\text{eq}})$ adapts the discontinuous control to the applicable values of $u \in \{-1, 0, 1\}$. Moreover, recovering (7) and replacing the proposed control, one gets

$$\dot{\sigma} = \frac{E\alpha}{2LC}\left(\text{sign}(u_{\text{eq}}) - \text{sign}(\sigma) - 2u_{\text{eq}}\right) \tag{11}$$

which can be rewritten as

$$\dot{\sigma} = \begin{cases} \frac{E\alpha}{2LC}\left(2|u_{eq}| - 1 - \text{sign}(\sigma)\right) & \text{when } u_{\text{eq}} < 0 \\ -\frac{E\alpha}{2LC}\text{sign}(\sigma) & \text{when } u_{\text{eq}} = 0 \\ \frac{E\alpha}{2LC}\left(1 - 2u_{eq} - \text{sign}(\sigma)\right) & \text{when } u_{\text{eq}} > 0 \end{cases} \tag{12}$$

and fulfils $\sigma\dot{\sigma} < 0$ for $-1 < u_{\text{eq}} < 1$.

### C. Ideal Sliding Mode Dynamics

Once the sliding mode is established with the proposed control law (10), the stability of the overall system should be checked. The dynamics of the output voltage is given by

$$e_v + \alpha\, \dot{e}_v = 0 \tag{13}$$

which provides $e_v \to 0$ when $\alpha > 0$, and, hence, is asymptotically stable and perfect tracking is achieved. The current dynamics is set by (2b) and can be analyzed for different loads as follows:

1) Resistive load: Equation (2b) yields $i_L = C\frac{dv_c}{dt} + \frac{v_c}{R}$, providing a bounded current resulting in $i_{Lss} = A(C\omega\cos(\omega t) + \frac{1}{R}\sin(\omega t))$ at steady-state.

2) Linear load with impedance $Z_o(s) = \frac{V_c(s)}{I_o(s)}$: In this case the inductor current is given by $I_L(s) = Z(s)V_c(s)$, where $Z(s) = (Cs + Z_o^{-1}(s))$, and stability can be determined from $Z(s)$.
3) Nonlinear load, $i_o = f(v_c)$: In such case, $i_L = C\frac{dv_c}{dt} + f(v_c)$. Stability depends on the function $f(v_c)$, so if $f(v_c)$ is bounded, the inductor current will also be delimited, but if $f(v_c)$ is not bounded, the inductor current will be unstable.

### D. Robustness Analysis

Assuming that switching surface has been designed to guarantee asymptotic stability of the sliding motion, the robustness of the control can be determined analysing the conditions that ensure the sliding mode regime. These conditions are given by the inequalities that define the sliding domain

$$-1 < u_{\text{eq}} = \frac{v_c}{E} + \frac{LC}{\alpha E}\left[\frac{\alpha}{C}\frac{di_o}{dt} - \dot{v}_c + \dot{v}_c^* + \alpha\ddot{v}_c^*\right] < 1 \quad (14)$$

which, since $i_o = f(v_c)$, can be rewritten as

$$-1 < \frac{v_c}{E} + \frac{LC}{\alpha E}\left[\left(\frac{\alpha}{C}\frac{df(v_c)}{dv_c} - 1\right)\dot{v}_c + \dot{v}_c^* + \alpha\ddot{v}_c^*\right] < 1. \quad (15)$$

Notice that a high value of $\frac{df(v_c)}{dv_c}$, for instance a sudden load change, can lead to a loss of the sliding regime. In this scenario, the control law should guarantee the recovery of the sliding motion.

Moreover, (15) should be fulfilled at steady-state, $v_c = v_c^*$. Therefore, assuming certain maximum value of the slope of $f(v_c)$ at steady-state, i.e., $dv_{c\max} = [\frac{df(v_c)}{dv_c}]_{\max}$, the sliding domain becomes

$$-1 < \frac{1}{E}\left(v_c^* + L\, dv_{c\max}\dot{v}_c^* + LC\,\ddot{v}_c^*\right) < 1 \quad (16)$$

which, replacing $v_c^* = A\sin\omega t$, can be written as

$$-1 < \frac{A}{E}\left(\left(1 - LC\,\omega^2\right)\sin\omega t + L\,\omega\, dv_{c\max}\cos\omega t\right) < 1. \quad (17)$$

From (17), it is straightforward to get the condition to be fulfilled to guarantee the sliding dynamics

$$\left|\frac{1}{\sqrt{\left(1 - LC\,\omega^2\right)^2 + \left(L\,\omega\, dv_{c\max}\right)^2}}\right| > \frac{A}{E}. \quad (18)$$

For the particular case when the VSI is loaded with a resistive load, $f(v_c) = \frac{v_c}{R}$, (18) can be expressed as

$$\left|\frac{1}{\sqrt{\left(1 - LC\,\omega^2\right)^2 + \left(\frac{L\,\omega}{R}\right)^2}}\right| > \frac{A}{E}. \quad (19)$$

## IV. Three-Level Sliding Mode Controller Implementation

When a FOSMC is implemented, the sign function is usually replaced by a comparator with hysteresis. The hysteresis band adjustment allows to limit the switching frequency. The dynamics that appears when hysteresis comparators are used instead of sign functions can be called real sliding dynamics. In the standard two-level FOSMC the replacement is easy and immediate, but when it comes to the three-level sliding mode controller the solution is not obvious. Note that the SMC law given in (10) requires the knowledge of the sign of the equivalent control, $\text{sign}(u_{\text{eq}})$. The equivalent control would place the switching function at $\sigma = 0$, and assumes (theoretically) infinite switching frequency. It depends on the variables and parameters of the system and therefore requires full system knowledge, which is impossible in practical applications. The most realistic approach is to low-pass filter the discontinuous control action enforced by the sliding mode, but the equivalent control would always be obtained with a delay or phase shift. As a result, the estimation of the sign of the equivalent control deserves special attention in order to properly implement (10). One option is to approximate the equivalent control to determine its sign. Using (6), an approximation is

$$u_{\text{eq}} \approx \frac{v_c^*}{E} \quad (20)$$

but in most cases can not be used in practice because the phase shifting between $v_c^*$ and $u_{\text{eq}}$.

### A. Detection of Equivalent Control Sign

This work proposes to indirectly obtain the equivalent control sign. Note that (12) splits the calculus of $\dot{\sigma}$ in two regions defined by $0 < u_{\text{eq}} < 1$ and $-1 < u_{\text{eq}} < 0$. Therefore, the evaluation of $\dot{\sigma}$ can provide information about the sign of the equivalent control. In fact, SMC law is designed to fulfil that $\dot{\sigma}\sigma < 0$; that is, the slope of $\sigma$ always points to the surface $\sigma = 0$. In other words, $\dot{\sigma} = 0$ indicates that the sliding motion is going to be lost. This is the property that is exploited in the three-level sliding mode implementation. In fact, the loss of sliding motion when operating with $u = 0$ is an expected scenario and requires to update the control signal from $u = \{0, 1\}$ to $u = \{-1, 0\}$ when $u_{\text{eq}}$ goes from positive to negative and viceversa to avoid it.

With this in mind, in order to implement the three-level control with a two-level hysteresis band comparator the control law (10) is modified as

$$u = \frac{1}{2}\left[u_{S_{\text{eq}}} - \nu\right] \quad (21)$$

that consists in the following two terms.

1) The first one replaces the sign of $u_{eq}$ in (10) and follows the abovementioned idea. The variable $u_{S_{\text{eq}}} \in \{-1, 1\}$ is defined as

$$u_{S_{\text{eq}}} = |u|\, u_{S_{\text{eq}}} - (1 - |u|)\ \text{sign}(\dot{\sigma}) \quad (22)$$

where the initial state of $u_{S_{\text{eq}}}$ is set using the sign of (20).

2) The second term of (21) is the update of the sign function to include a hysteresis band, $\Delta$, see [1] for further details. The variable $\nu \in \{-1, 1\}$ is defined as

$$\nu = \text{sign}(\sigma + \Delta\,\nu). \quad (23)$$

Fig. 2 shows the scheme of the VSI with the three-level FOSMC and Fig. 3

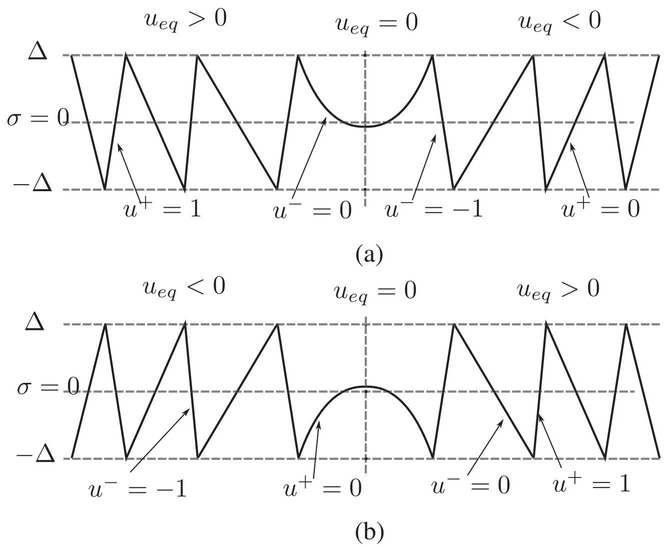


Fig. 3. Behavior of the switching function with the proposed three-level control. (a) From positive to negative $u_{\mathrm{eq}}$. (b) Viceversa.

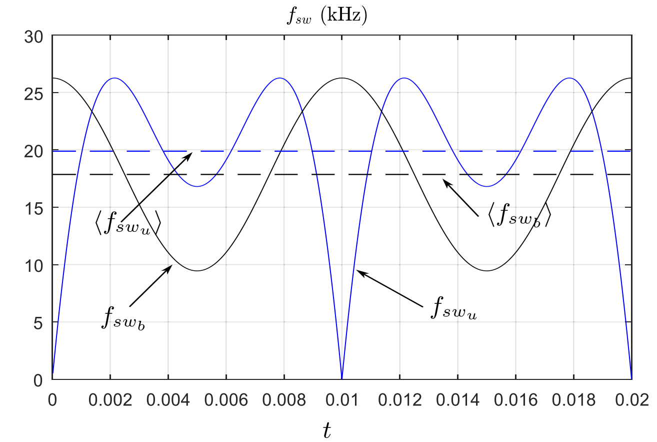


Fig. 4. Steady-state switching frequencies for two-level and three-level FOSMC in a reference signal period.

depicts the behavior of the switching function with the proposed controller in (21). As expected, it remains within the hysteresis band and the error is bounded.

### *B. Switching Frequency Analysis*

According to Fig. 3, it is possible to estimate the switching period of the control action $u$. Assuming a piecewise linear behavior inside the hysteresis band the switching period can be computed as

$$t_{\mathrm{sw}} = \frac{2\Delta}{\dot{\sigma}_+} - \frac{2\Delta}{\dot{\sigma}_-} \tag{24}$$

where $\dot{\sigma}_+$ and $\dot{\sigma}_-$ hold for the positive and negative switching function slopes within the hysteresis band, respectively. In the following, (24) is evaluated for two-level and three-level cases as follows:

1) When SMC is implemented using two-level signal, i.e., $u \in \{-1, 1\}$, replacing (7) in (24) yields

$$t_{\mathrm{sw}_b} = \frac{4\Delta_b LC}{\alpha E}\left[\frac{1}{1 - {u_{\mathrm{eq}}}^2}\right] \tag{25}$$

where $\Delta_b$ is the hysteresis band of the comparator. The switching frequency can be estimated as

$$f_{\mathrm{sw}_b} = \frac{\alpha E}{4\Delta_b LC}\left[1 - {u_{\mathrm{eq}}}^2\right]. \tag{26}$$

2) For the three-level case, considering (12), (24) can be computed when the equivalent control is positive

$$t_{\mathrm{sw}_u} = \frac{2\Delta_u LC}{\alpha E\,(1 - u_{\mathrm{eq}})} + \frac{2\Delta_u LC}{\alpha E\, u_{\mathrm{eq}}} \tag{27}$$

and when the equivalent control is negative

$$t_{\mathrm{sw}_u} = -\frac{2\Delta_u LC}{\alpha E u_{\mathrm{eq}}} + \frac{2\Delta_u LC}{\alpha E\,(1 + u_{\mathrm{eq}})} \tag{28}$$

which can be merged in

$$t_{\mathrm{sw}_u} = \frac{2\Delta_u LC}{\alpha E}\frac{1}{|u_{\mathrm{eq}}| - {u_{\mathrm{eq}}}^2}. \tag{29}$$

Therefore, the switching frequency can be obtained as

$$f_{\mathrm{sw}_u} = \frac{\alpha E}{2\Delta_u LC}\left(|u_{\mathrm{eq}}| - {u_{\mathrm{eq}}}^2\right). \tag{30}$$

The steady-state averaged values of the switching frequency in both cases can also be found using (26) and (30). From (6), and noticing that at steady-state $v_c = v_c^*$, the steady-state equivalent control is

$$u_{mss} = B\sin(\omega t + \theta) \tag{31}$$

where

$$B = \frac{A}{E}\sqrt{(1 - LC\omega^2)^2 + \left(\frac{L}{R}\omega\right)^2} \tag{32}$$

and

$$\theta = \arctan\left(\frac{L\omega}{R\,(1 - LC\omega^2)}\right). \tag{33}$$

Therefore, replacing (31) in (26) and (30) and applying the operator

$$\langle f_{\mathrm{sw}}\rangle = \frac{1}{T}\int_0^T f_{\mathrm{sw}}\, dt$$

to the $f_{\mathrm{sw}_b}$ and $f_{\mathrm{sw}_u}$, the steady-state averaged switching frequency results in

$$\langle f_{\mathrm{sw}_b}\rangle = \frac{\alpha E}{4\Delta_b LC}\left(1 - \frac{B^2}{2}\right) \tag{34}$$

for the two-level case, and

$$\langle f_{\mathrm{sw}_u}\rangle = \frac{\alpha E}{2\Delta_u LC}\left(\frac{2B}{\pi} - \frac{B^2}{2}\right) \tag{35}$$

for the three-level one.

Fig. 4 shows the plot of the expressions (26), (30), (34), and (35) using the data of Table I but setting the hysteresis band

TABLE I
VSI AND FOSMC PARAMETERS

| Parameter | Symbol | Value |
|---|---|---|
| Input voltage | $E$ | 420 V |
| Reference signal | $v_c^*(t)$ | $220\sqrt{2}\sin(2\pi 50t)$ V |
| Output voltage frequency | $f$ | 50 Hz |
| Inductor | $L$ | 400 $\mu$H |
| Capacitor | $C$ | 50 $\mu$F |
| Output power | $P$ | 1.2 kW |
| FOSMC parameter | $\alpha$ | 0.005 |
| Hysteresis band two-levels | $\Delta_b$ | 954 |
| Hysteresis band three-levels | $\Delta_u$ | 518 |
| Dead time | | 1 $\mu$s |

values to $\Delta_u = 500$ and $\Delta_b = 1000$. The value of the equivalent control amplitude is of $B = 0.7393$. It is straightforward to obtain the values of the time instants when the switching frequency functions get their maximums and minimums within the signal period. That is, two maximums of

$$f_{\text{swb}_{\max}} = \frac{\alpha E}{4\Delta_b LC} \tag{36}$$

at $t_1 = \frac{1}{\omega}(\pi - \theta)$ and $t_2 = \frac{1}{\omega}(2\pi - \theta)$, and two minimums of

$$f_{\text{swb}_{\min}} = \frac{\alpha E}{4\Delta_b LC}\left(1 - B^2\right) \tag{37}$$

at $t_1 = \frac{1}{2\omega}(\pi - 2\theta)$ and $t_2 = \frac{1}{2\omega}(3\pi - 2\theta)$ for the two-level case. With respect the three-level case, the corresponding values are

$$f_{\text{swu}_{\max}} = \frac{\alpha E}{8\Delta_u LC} \tag{38}$$

for $t_1 = \frac{1}{\omega}(\phi - \theta)$, $t_2 = \frac{1}{\omega}(\pi - \phi - \theta)$, $t_3 = \frac{1}{\omega}(\pi + \phi - \theta)$, and $t_4 = \frac{1}{\omega}(2\pi - \phi - \theta)$, where $\phi = \arcsin(\frac{1}{2B})$, for the maximum and takes the minimum value of zero at $t_1 = \frac{1}{\omega}(\pi - \theta)$ and $t_2 = \frac{1}{\omega}(2\pi - \theta)$. The plot of Fig. 4 displays all these maximums and minimums, including the zero minimum of the three-level case, which means that the sliding motion is momentarily lost. Furthermore, the figure also shows the switching frequency averaged values obtained using (34) and (35), which have been plotted with dashed lines. Notice that for the given values of $\Delta_b$ and $\Delta_u$ the values do not match. Both FOSM controllers can operate with the same average switching frequency when $\Delta_b$ and $\Delta_u$ are set in compliance with the expression

$$\frac{\Delta_u}{\Delta_b} = \frac{B\,(8 - 2\pi B)}{\pi(2 - B^2)} \tag{39}$$

which is obtained equaling (34) and (35).

From (39), and with $B = 0.7393$, it can be deduced that $\Delta_u = 0.5432\Delta_b$ ensures the same averaged switching frequency for both FOSM, which results in $\Delta_b = 954$ and $\Delta_u = 518$ for 20 kHz with the parameters shown in the Table I.

*Remark 1:* When the three-level FOSM and the two-level FOSM operate at the same switching frequency, the current

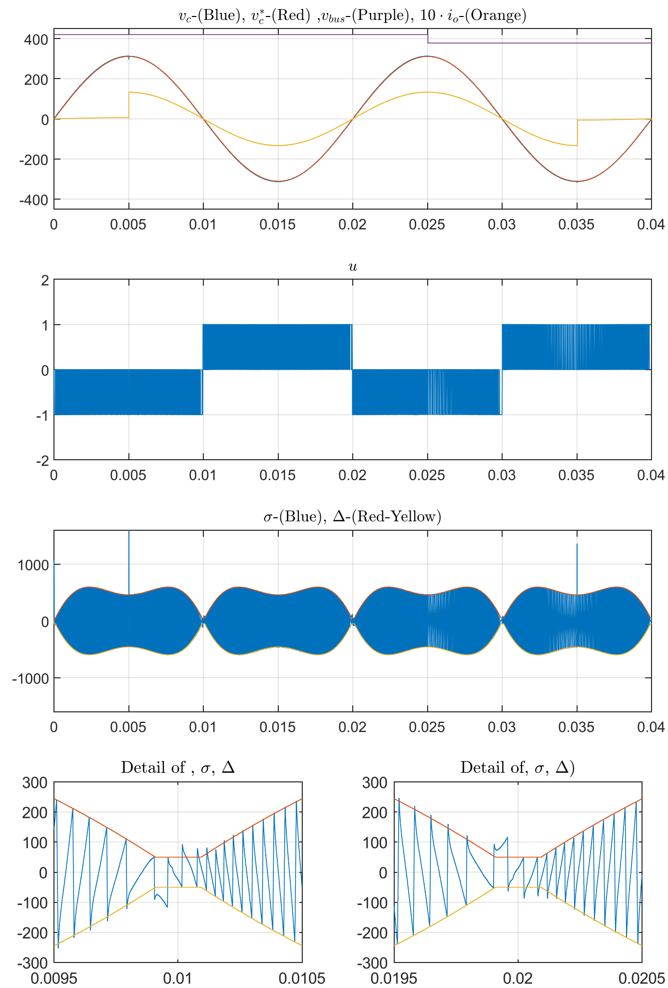


Fig. 5. From top to bottom. 1—Output voltage, reference voltage, bus voltage, and output current. 2—Control action. 3—Switching function and hysteresis band. 4—Details of switching function and hysteresis band.

ripple of the former is lower than that of the latter. That is, from the state equations shown in (2) and assuming that $v_c \geq 0$, it is straightforward to find that the current ripple of the three-level and second-level approaches are given by

$$\Delta i_{Lu} = \frac{1}{L}\,(E - v_c)\,\frac{v_c}{E} t_{\text{sw}} \tag{40}$$

and

$$\Delta i_{Lb} = \frac{1}{2L}\,(E - v_c)\left(1 + \frac{v_c}{E}\right) t_{\text{sw}} \tag{41}$$

respectively. Hence, the ratio between the ripples is

$$\frac{\Delta i_{Lu}}{\Delta i_{Lb}} = \frac{2v_c}{E + v_c} \tag{42}$$

which, since the single-phase inverter is a step-down converter, is always less than unity. The Fig. 8

shows the graph of the evolution of the current ripple ratio within the positive half-period of the output voltage.

TABLE II
EXPERIMENTAL RESULTS OF THE VSI

| Hysteresis | Output Power (kW) | THD Voltage (%) | | Voltage error (%) | |
|---|---|---|---|---|---|
| | | Two-level | Three-level | Two-level | Three-level |
| Linear Load | | | | | |
| Variable | 0 | 0.2 | 0.4 | 0.74 | 1.79 |
| Fixed | 1.2 | 0.2 | 0.7 | 0.77 | 2.03 |
| Variable | 1.2 | 0.2 | 0.4 | 0.74 | 1.79 |
| Nonlinear Load | | | | | |
| Fixed | 0.63 | 0.3 | 0.9 | 1.73 | 2.12 |
| Variable | 0.63 | 0.2 | 0.4 | 1.60 | 2.05 |

* Measured with a FLUKE 434 Power quality analyzer.

TABLE III
FIGURES OF MERIT OF UNIPOLAR SMC SINGLE-PHASE INVERTERS

| | $E$ | $v_c$ | $f_{sw}$ | $C$ | $L$ | Power | THD (L) | THD (NL) | Transient time | Controller |
|---|---|---|---|---|---|---|---|---|---|---|
| This work | 420 V | 220 $V_{\text{rms}}$ | 20 kHz | 100 $\mu$F | 0.4 mH | 1.2 kW | 0.7 % | 0.9 % | 0.3 ms | SMC with symmetrical two-level hyst. |
| [19] | 275 V | 120 $V_{\text{rms}}$ | 13.42 kHz | 100 $\mu$F | 0.25 mH | 0.48 kW | 0.74$^\star$ % | 3.4 % | - | SMC with three-level hyst. |
| [17] | 300 V | $\frac{200}{\sqrt{2}}$ $V_{\text{rms}}$ | 21.67 kHz | 100 $\mu$F | 0.25 mH | 1.6 kW | 1.9 % | - | 0.2 ms | Fuzzy logic + SMC with three-level hyst. |
| [8] | 360 V | 220 $V_{\text{rms}}$ | 15 kHz | 9.4 $\mu$F | 0.357 mH | 6 kVA | 1.1 % | 1.7 % | 0.5 ms | PWM with boundary layer SMC |

$\star$ Simulation result.

### *C. Variable Hysteresis Band for Bounded Switching Frequency Operation*

Switching frequency can be set to a desired value, $t^d_{\text{sw}_u}$, adjusting the hysteresis band using (29). That is, from (29), one gets

$$\Delta_u = \frac{\alpha E}{2LC} t^d_{\text{sw}_u} \left(|u_{\text{eq}}| - {u_{\text{eq}}}^2\right) \tag{43}$$

which, evaluated at steady-state and considering (31), can be written as

$$\Delta_u = \frac{\alpha EB}{2LC} t^d_{sw_u} \left(|\sin(\omega t + \theta)| - B\sin^2(\omega t + \theta)\right) \tag{44}$$

where $B$ and $\theta$ have been defined in (32) and (33), respectively. Notice that the hysteresis nullifies periodically when $\omega t + \theta = k\pi$, $k \in \mathbb{Z}$. In order to ensure a nonzero hysteresis value at any time, $\Delta_u$ is saturated to a small (close to zero) value.

### *D. Simulation Results*

In order to test the proposed three-level FOSMC, a VSI with parameters shown in the Table I was numerically simulated using Matlab–Simulink software. The power stage was built with the Simscape toolbox and the controller was implemented using Simulink blocks. The solver was the discrete (no continous states) and the simulation step was a fixed-step of 20 ns. The switching frequency was set to 20 kHz. The discrete-time simulation was carried out including nonideal effects (losses, dead times,...) and discretization issues, such as computational delay or the resolution of the PWMs and the ADCs. The results confirm the expected good performance of the controlled VSI for the following cases.

1) When facing load and input voltage variations (see Fig. 5). Specifically, the load changes from open circuit to 24 Ω, and viceversa, and the input voltage does so from 420 to 380 V.
2) When the VSI is been loaded with a diode rectifier acting as a nonlinear load (see Fig. 6).
3) When there are $\pm 50$ % variations in capacitor and inductor values with a load transient from no load to 22 Ω (see Fig. 7).

In addition, to the good behavior of the VSI output voltage, the simulations also show several important facts to be remarked as follows:

1) The eventually loss of the sliding regime due to the sudden load change (see third subplot of Fig. 5) as it was pointed out in Section III-D.
2) The behavior of the switching functions when the control changes from the $\{-1, 0\}$ set to $\{0, 1\}$ set (see bottom subplots of Figs. 5 and 6). Notice that, due to the small values of the switching surface, the voltage error is also lower than the fixed hysteresis case one, thus reducing the output voltage THD. Moreover, since the simulation includes the computing delays and the hysteresis band takes its minimum value, eventually the switching function evolves out of the hysteresis bands.
3) The controller shows high robustness when faced with output $LC$ filter variations. Notice that the sliding motion is preserved in all the simulated cases shown in Fig. 7.

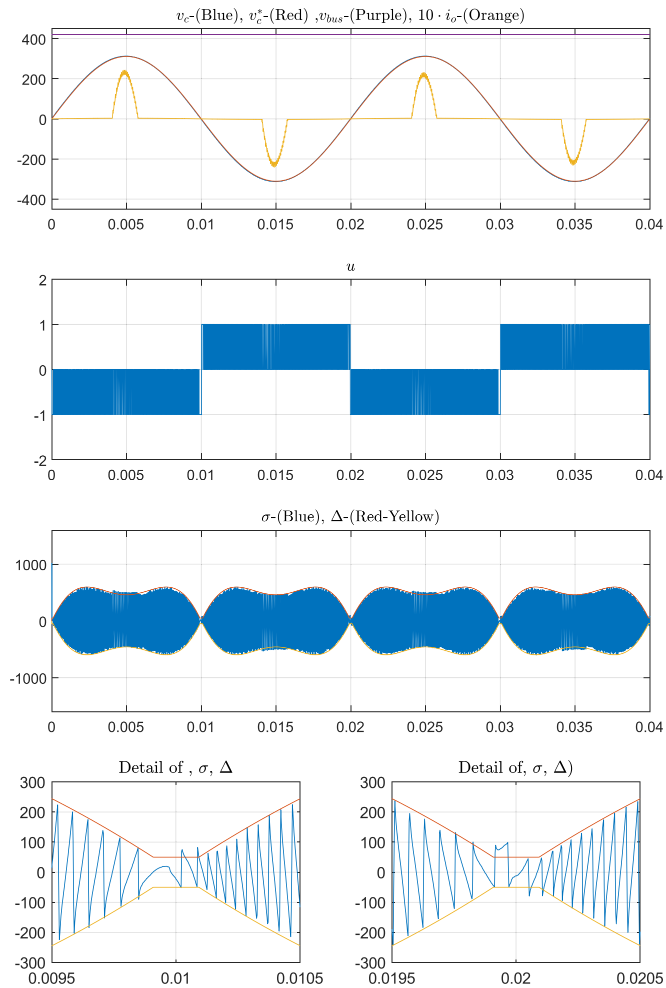


Fig. 6. From top to bottom. 1—Output voltage, reference voltage, bus voltage, and output current. 2—Control action. 3—Switching function and hysteresis band. 4—Details of switching function and hysteresis band.

Furthermore, switching frequency evolution has also been numerically calculated from the simulation data and it is shown in Fig. 9
for fixed hysteresis operation and when the hysteresis is dynamically adapted. As expected, the results confirm that variations of the switching frequency around the desired value are reduced in the last case.

## V. Implementation Details

The three-level FOSCMC has been implemented using the TMS320F28377S microcontroller ($\mu$C) from Texas Instruments and it has been experimentally evaluated.

### A. Experimental Setup

Table I shows the VSI parameters of the setup. For the VSI full-bridge, the switch IGBT 50MT060WTHA has been used. The output capacitor is formed by two capacitors C4AEGBW5500A3LJ connected in parallel ($2 \times 50$ $\mu$F). The inductor has been built using gapped ferrite cores wound with copper litz wire. The time derivative of the output voltage is obtained measuring the output capacitor current with a hand-wound current transformer (CT). The number of turns is 500, resulting in a secondary inductance of 800 mH. The secondary of the CT is closed by a burden resistor of 6.8 Ω.

### B. Controller Discretization

The controller and the hysteresis band adaptation algorithms have been programmed in the TMS320F28377S $\mu$C. Details concerning the implementation are described in the following.

*1) Digital Implementation of the FOSMC:* In this work, the approach used to implement the controller consists of emulating the behaviour of a continuous-time hysteresis comparator in a discrete-time domain. This technique was also applied in [15] and [16]. It can be summarized as follows:

1) The switching function is computed at any sampling period according to (4) through the ADC's of the $\mu C$. At sampling instant $k$, $\sigma_k$ is computed.
2) Once the switching function is computed, a prediction of the $k+2$ sample is calculated, assuming piecewise linear behavior of $\sigma$. Then, $\hat{\sigma}_{k+2}$ is obtained at time instant $kT$ as

$$\hat{\sigma}_{k+2} = 3\sigma_k - 2\sigma_{k-1}. \tag{45}$$

3) The emulation of the hysteresis comparator is performed using a PWM, as shown in Fig. 10. According to the figure, the control action must be able to switch from 0 to 1 at $t = t_1 + 2kT$. Then, the duty cycle, $d$, of $u$ to be loaded at $t = 2kT$ is

$$d_k = \frac{T - t_1}{T} = \frac{\hat{\sigma}_{k+2} - \Delta}{\hat{\sigma}_{k+2} - \hat{\sigma}_{k+1}}. \tag{46}$$

The computing delay, $t_c$, produces that the computed control signal at $kT$ cannot be loaded until $2kT$. This justifies the prediction of $\hat{\sigma}_{k+2}$ for obtaining an approximated behavior of the ideal hysteresis comparator. With that technique, the computing delay effect is bypassed.
4) The expression for computing $d$ when $u$ switch from 1 to 0 is

$$d_k = \frac{t_2}{T} = \frac{-\Delta - \hat{\sigma}_{k+4}}{\hat{\sigma}_{k+5} - \hat{\sigma}_{k+4}}. \tag{47}$$

The proposed idea for implementing the hysteresis comparator using a discretized system works as expected as the piecewise linear behavior hypothesis is fulfilled. As a consequence, the algorithm runs as fast as possible, in this case at $T = 1.6$ $\mu s$. This sampling time has been made possible by the ability of parallel code execution through the control law accelerator (CLA), which is another processor included in the F28377s. Basically, the control code is executed in the CLA, meanwhile the main CPU is in charge of generating the voltage reference, writing in the DAC registers for visualization, checking possible over-currents, communications with the host PC, etc. A block diagram of the implementation is shown in Fig. 11.

*2) Hysteresis Band Adaptation:* The hysteresis band is adjusted using (43), which has been discretized and programmed in the $\mu C$. The value of the equivalent control of (43) has

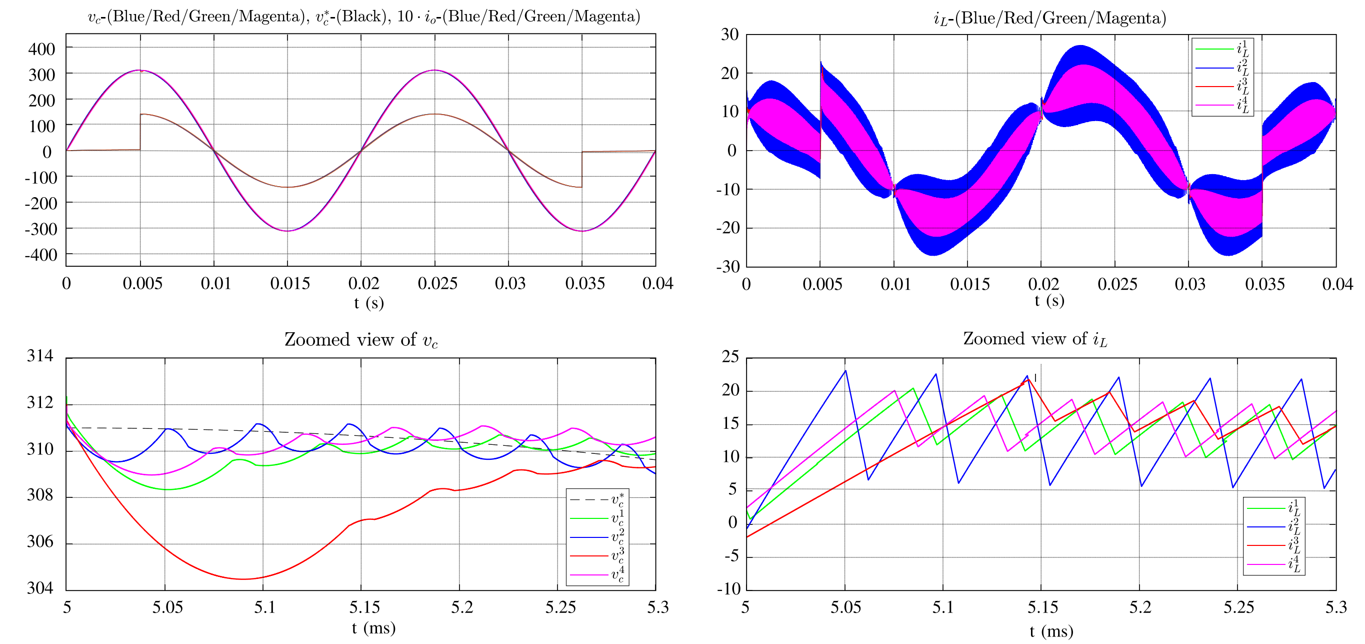


Fig. 7. Load transient (No load to 22 Ω). Case 1 (green): Nominal values. Case 2 (blue): $L = 220\ \mu H$ and $C = 150\ \mu F$. Case 3 (red): $L = 660\ \mu H$, and $C = 100\ \mu F$. Case 4 (magenta): $L = 440\ \mu H$, and $C = 50\ \mu F$. Left-top plot: $v_c$ and $i_o$. Right-top plot: $i_L$. Bottom plots: Zoomed views of the load transient.

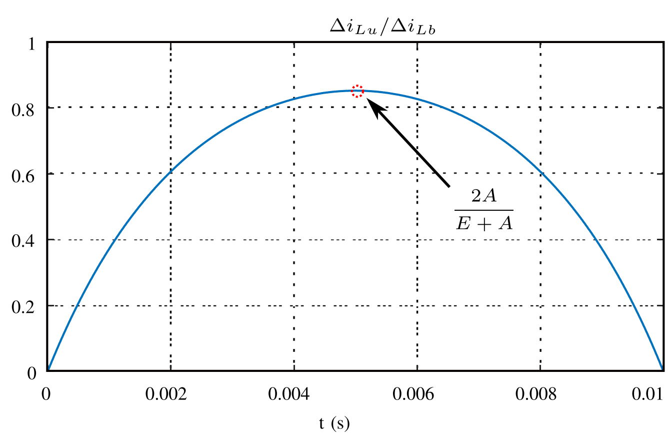


Fig. 8. Current ripple ratio for a single-phase inverter with the parameters shown in the Table I.

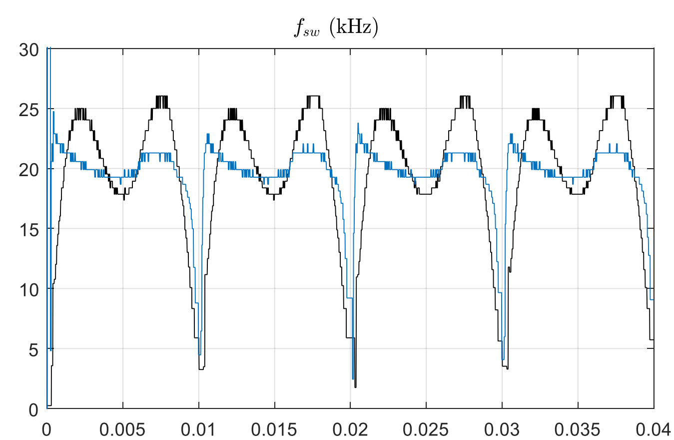


Fig. 9. Switching frequency behavior for three-level operation using fixed (black) or variable (blue) hysteresis bands.

been approximated to $u_{\text{eq}} = \frac{v_c^*}{E}$ and the minimum value of the hysteresis band has been set to $\Delta_{\text{min}} = 50$.

## VI. Experimental Results

In order to highlight the differences between the standard two-level approach and the proposed three-level FOSMC, the controllers have been tested under the same working scenarios. The results are detailed in the following sections.

### A. Test 1: Steady-State Behavior

The first tests consist of operating the FOSMCs with a constant hysteresis band. Fig. 12 shows the steady-state converter variables for the two-level case and Fig. 13 those for the three-level one. Noticed how the control signal is modulated by the switching function behaving within the hysteresis band. In the two-level case, the duty cycle varies from maximum to minimum, around the capacitor voltage peaks, achieving a value of 0.5 when the capacitor voltage is close to changing polarity. As expected, the behaviour of the switching function for the three-level case is quite different. When reaching the change of polarity, the slope of the switching surface tends to become zero, meaning that the sliding regime is close to be lost. At this point, the controller acts and changes the control thus avoiding the loss of the sliding motion and retaining the switching surface within the hysteresis band. Figs. 14 and 15 show the steady-state variables for the two-level and three-level case, respectively, when the hysteresis bands are dynamically

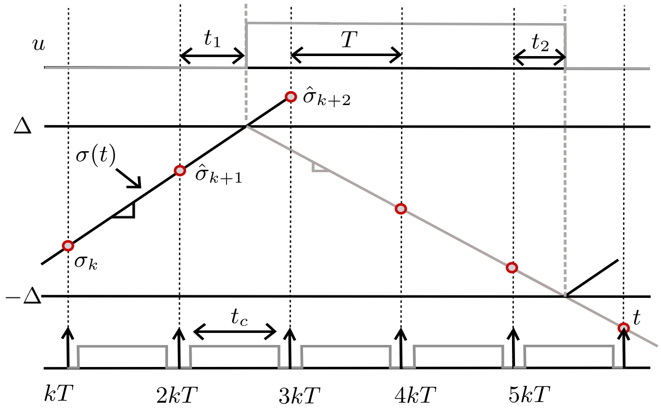


Fig. 10. Emulation of a continuous-time hysteresis comparator in a discrete-time domain.

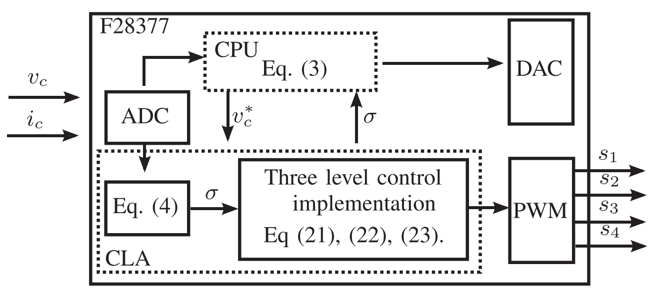


Fig. 11. Block diagram of the peripheral used for the implementation of the FOSMC in the TMS320F28377S $\mu$C.

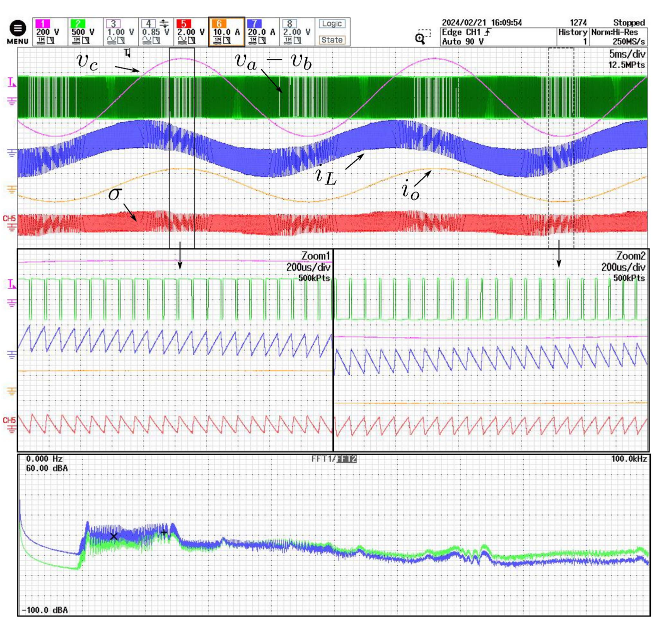


Fig. 12. Two-level. Steady-state VSI response with fixed hysteresis band and $R = 44\Omega$. From top to bottom: $v_c$ (magenta); $v_a - v_b$ (green); $i_L$ (purple); $i_o$ (orange) and $\sigma$ (red). Middle plots: zoom views; bottom plot: FFT of $v_a - v_b$ and $i_L$.

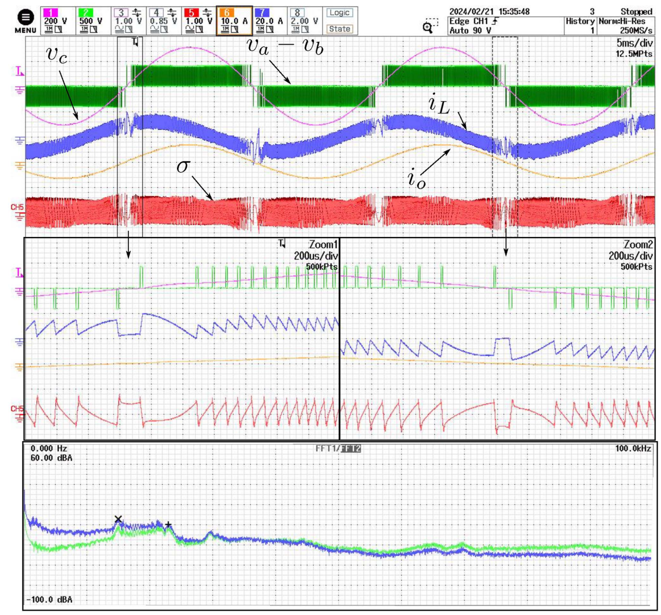


Fig. 13. Three-level. Steady-state VSI response with fixed hysteresis band and $R = 44\Omega$. From top to bottom: $v_c$ (magenta), $v_a - v_b$ (green), $i_L$ (purple), $i_o$ (orange), and $\sigma$ (red). Middle plots: zoom views and bottom plot: FFT of $v_a - v_b$ and $i_L$.

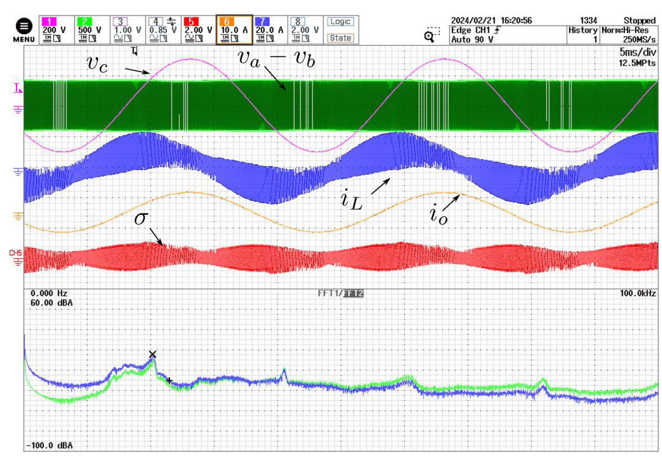


Fig. 14. Two-level. Steady-state VSI response with variable hysteresis band and $R = 44\Omega$. From top to bottom: $v_c$ (magenta), $v_a - v_b$ (green), $i_L$ (purple), $i_o$ (orange), and $\sigma$ (red). Bottom plot: FFT of $v_a - v_b$ and $i_L$.

adapted to bound the switching frequency around 20 kHz. The FFTs of the inductor current and the control voltage have also been included. By comparing the FFTs of Figs. 14 and 15 with their corresponding in Figs. 12 and 13, one can easily check how the switching frequency spread is lowered when hysteresis adaptation is applied.

### B. Test 2: Diode-Rectifier Load

A diode rectifier with parameters $R_L = 150\,\Omega$, $r_s = 1\,\Omega$, and $C_L = 6.6$ mF, providing a crest factor of 3 with a current peak of 14 A for an output voltage amplitude of $220\sqrt{2}$ V, has been used as nonlinear load for the test. Figs. 16 and 17 present the

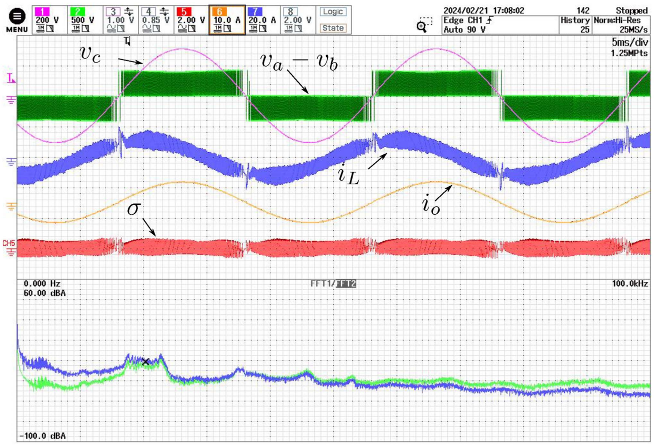


Fig. 15. Three-level. Steady-state VSI response with variable hysteresis band and $R = 44\Omega$. From top to bottom: $v_c$ (magenta); $v_a - v_b$ (green), $i_L$ (purple), $i_o$ (orange), and $\sigma$ (red). Bottom plot: FFT of $v_a - v_b$ and $i_L$.

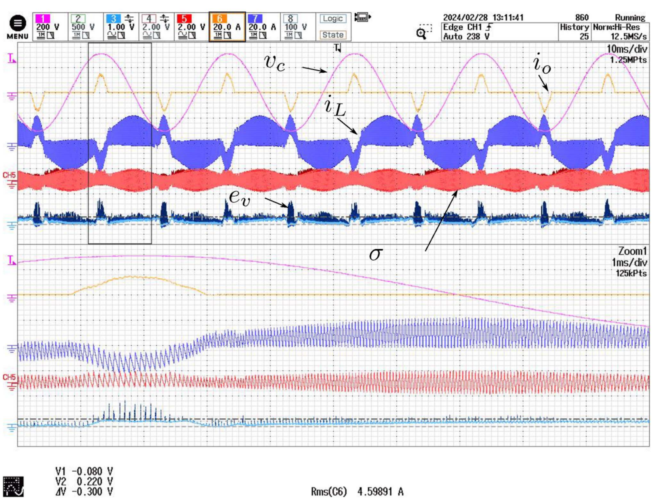


Fig. 16. Two-level. Steady state with a diode rectifier. From top to bottom: $v_c$ (magenta), $i_o$ (orange), $i_L$ (purple), $e_v$ (blue), $i_o$ (orange), and $\sigma$ (red).

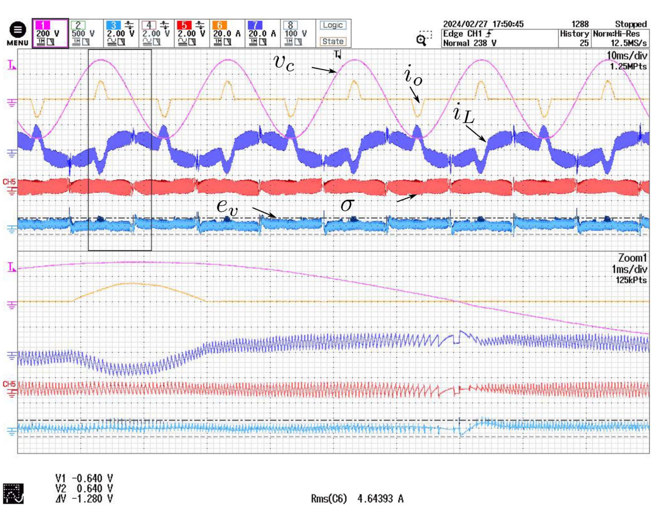


Fig. 17. Three-level. Steady state with a diode rectifier. From top to bottom: $v_c$ (magenta), $i_o$ (orange), $i_L$ (purple), $e_v$ (blue), $i_o$ (orange), and $\sigma$ (red).

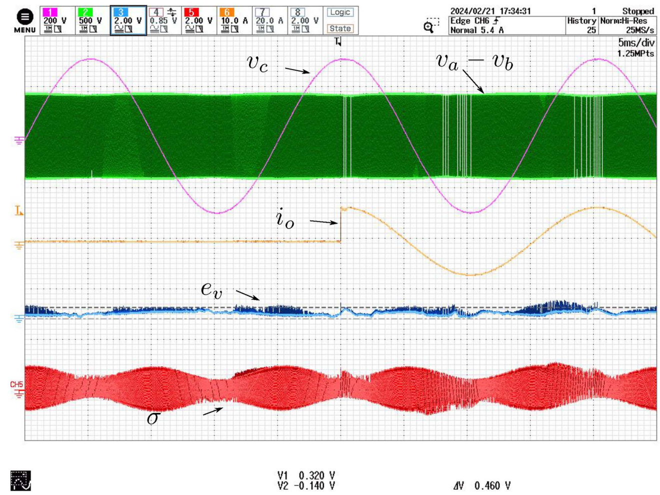


Fig. 18. Two-level. VSI transient response from no load to $R = 44\Omega$. From top to bottom: $v_c$ (magenta), $v_a - v_b$ (green), $e_v$ (blue); $i_o$ (orange), and $\sigma$ (red).

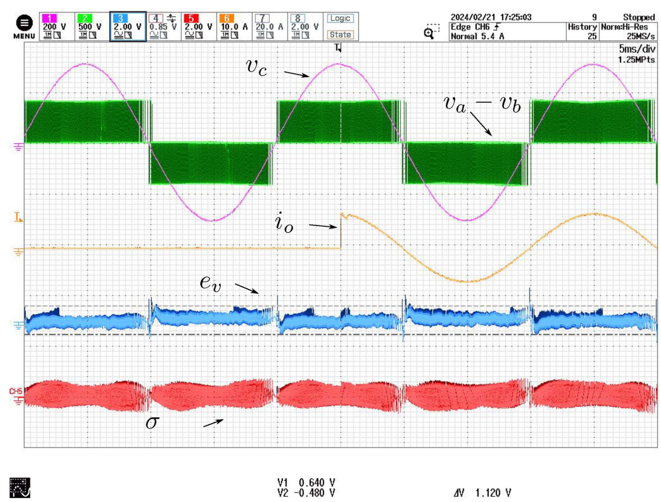


Fig. 19. Three-level. VSI transient response from no load to $R = 44\Omega$. From top to bottom: $v_c$ (magenta), $v_a - v_b$ (green), $e_v$ (blue), $i_o$ (orange), and $\sigma$ (red).

results for the two-level and three-level case, respectively. Both figures also show the voltage error, and the peak-to-peak values of $e_v = 10$ V and $e_v = 12.8$ V can be measured, which results in a 1.60 %, for the two-level case, and a 2.05 %, for the three-level one, with respect to the peak-to-peak output voltage. Note that, although the error in the three-level case is higher than the value of the two-level case, this value is still good for such nonlinear load.

## C. Test 3: Output Voltage Regulation

The VSI has also been tested when the load changes from open circuit to 44 Ω. The transient responses can be seen in Figs. 18 and 19. Note that the transient has been produced in the worst case, where the peak current is maximum. In both cases, the switching function does not leave the hysteresis band, the transient is very fast and the voltage error remains the same with a peak-to-peak values of $e_v = 4.6$ V and $e_v = 11.2$ V, for the two-level case and the three-level one, respectively.

### D. Test 4: THD

The THD and maximum voltage tracking error are shown in the Table II. These data confirm the good performance of both implementations in sliding mode. For both indexes, the two-level sliding controller shows smaller values than the three-level one, but it should be remembered that the three-level implementation provides a lower current ripple for the same switching frequency. On the other hand, the comparison of the THD data for fixed and variable hysteresis confirms, as expected in both cases, two and three levels, that the use of dynamic hysteresis band adaptation results in a lower THD value.

## VII. Comparative Analysis

The control algorithm has been compared with three-level SMC reported in the specialist literature. Table III shows the main figures of merit for the proposed SMC implemented with a symmetric two-level hysteresis comparator, a SMC with three-level hysteresis comparator implemented as two level hysteresis functions [19], the extension of the previous work with a fuzzy logic adaptation to improve the transient response [17], and in [8] where the SMC is implemented using a boundary layer and fixed-frequency operation is obtained with a PWM. Note that the proposed SMC achieves the best THD indexes with both linear and nonlinear loads. Moreover, regarding the transient time after a load change, it should be remarked that fastest response corresponds to the design of a rotating-sliding-line-based SMC particulary developed for an enhaced transient but using fuzzy logic that complicates the implementation of the controller. The present proposal shows also very good transient response with a simple implementation.

## VIII. Conclusion

This article presents the implementation of a three-level (unipolar) FOSMC for a single-phase inverter. The controller is implemented using a single two-level hysteresis band comparator, which ensures that the switching function behaves within a symmetrical hysteresis centered at zero. The proposed design guarantees tracking of the reference sinusoidal voltage with robust behavior in the face of load and input voltage variations, as well as good measured performance in terms of error and harmonic distortion of the output voltage. In addition, the application of a variable hysteresis band provides a desired average switching frequency with a small frequency variation. A comparative experimental evaluation between the three-level and the two-level SMC with fixed and variable hysteresis band shows, as expected, that the former has lower ripple in the converter variables than the latter for the same switching frequency, and the THD and output voltage error are very low for linear and nonlinear load in all cases, being slightly better for the two-level variable hysteresis implementation than for the three-level case.

## References


[1] V. Utkin, J. Guldner, and J. Shi, *Sliding Mode Control in Electro-Mechanical Systems*, Boca Raton, FL, USA: CRC Press, 2009, vol. 34.

[2] R. W. Erickson and D. Maksimovic, *Fundamentals of Power Electronics.*, Cham, Switzerland, Springer Science & Business Media, 2007.

[3] R. R. Ramos, D. Biel, E. Fossas, and F. Guinjoan, "A fixed-frequency quasi-sliding control algorithm: Application to power inverters design by means of FPGA implementation," *IEEE Trans. Power Electron.*, vol. 18, no. 1, pp. 344–355, Jan. 2003.

[4] W. Qi, S. Li, S.-C. Tan, and S. R. Hui, "A constant-frequency parabolic-modulation-based sliding mode controller for buck converters," in *Proc. IEEE Appl. Power Electron. Conf. Expo.*, 2017, pp. 2010–2014.

[5] G. Balta, Ç. Hisar, and N. Altin, "Artificial intelligence based switching frequency regulation with fast terminal sliding mode control for DC–DC step-down converters," *Expert Syst. Appl.*, vol. 228, 2023, Art. no. 120331.

[6] G. Balta, N. Altin, and A. Nasiri, "Interval type-2 fuzzy-logic-based constant switching frequency control of a sliding-mode-controlled DC–DC boost converter," *Appl. Sci.*, vol. 13, no. 5, 2023, Art. no. 3239.

[7] S.-C. Tan, Y. Lai, C. K. Tse, and M. K. Cheung, "A fixed-frequency pulsewidth modulation based quasi-sliding-mode controller for buck converters," *IEEE Trans. Power Electron.*, vol. 20, no. 6, pp. 1379–1392, Nov. 2005.

[8] A. Abrishamifar, A. Ahmad, and M. Mohamadian, "Fixed switching frequency sliding mode control for single-phase unipolar inverters," *IEEE Trans. Power Electron.*, vol. 27, no. 5, pp. 2507–2514, May 2011.

[9] J. Ye, P. Malysz, and A. Emadi, "A fixed-switching-frequency integral sliding mode current controller for switched reluctance motor drives," *IEEE Trans. Emerg. Sel. Topics Power Electron.*, vol. 3, no. 2, pp. 381–394, Jun. 2015.

[10] P. A. Hosseinabadi, S. Mekhilef, H. R. Pota, and M. Kermadi, "Chattering-free fixed-time robust sliding mode controller for grid-connected inverters under parameter variations," *IEEE Trans. Emerg. Sel. Topics Power Electron.*, vol. 12, no. 1, pp. 579–592, Feb. 2024.

[11] C. Fu, C. Zhang, G. Zhang, and Z. Zhang, "Current sensorless sliding-mode voltage control for $LC$ filtered three-level T-type inverters," *IEEE Trans. Circuits Syst. II: Exp. Briefs*, vol. 71, no. 4, pp. 2264–2268, Apr. 2024.

[12] L. Zheng, F. Jiang, J. Song, Y. Gao, and M. Tian, "A discrete-time repetitive sliding mode control for voltage source inverters," *IEEE J. Emerg. Sel. Top. Power Electron.*, vol. 6, no. 3, pp. 1553–1566, Sep. 2018.

[13] W.-T. Yan, C. N.-M. Ho, H. S.-H. Chung, and K. T. Au, "Fixed-frequency boundary control of buck converter with second-order switching surface," *IEEE Trans. Power Electron.*, vol. 24, no. 9, pp. 2193–2201, Sep. 2009.

[14] V. Repecho, D. Biel, J. M. Olm, and E. F. Colet, "Switching frequency regulation in sliding mode control by a hysteresis band controller," *IEEE Trans. Power Electron.*, vol. 32, no. 2, pp. 1557–1569, Feb. 2017.

[15] V. Repecho, D. Biel, and J. M. Olm, "A simple switching-frequency-regulated sliding-mode controller for a VSI with a full digital implementation," *IEEE Trans. Emerg. Sel. Top. Power Electron.*, vol. 9, no. 1, pp. 569–579, Feb. 2021.

[16] V. Repecho, D. Biel, and A. Arias, "Fixed switching period discrete-time sliding mode current control of a PMSM," *IEEE Trans. Ind. Electron.*, vol. 65, no. 3, pp. 2039–2048, Mar. 2018.

[17] H. Komurcugil, "Rotating-sliding-line-based sliding-mode control for single-phase UPS inverters," *IEEE Trans. Ind. Electron.*, vol. 59, no. 10, pp. 3719–3726, Oct. 2012.

[18] H. Komurcugil, S. Ozdemir, I. Sefa, N. Altin, and O. Kukrer, "Sliding-mode control for single-phase grid-connected $LCL$-filtered VSI with double-band hysteresis scheme," *IEEE Trans. Ind. Electron.*, vol. 63, no. 2, pp. 864–873, Feb. 2016.

[19] O. Kukrer, H. Komurcugil, and A. Doganalp, "A three-level hysteresis function approach to the sliding-mode control of single-phase UPS inverters," *IEEE Trans. Ind. Electron.*, vol. 56, no. 9, pp. 3477–3486, Sep. 2009.

[20] M. di Benedetto, A. Faro, L. Bigarelli, A. Lidozzi, and L. Solero, "Constant delay-line frequency adaptive repetitive-resonant control for grid-tied and intentional islanding operations," *IEEE Trans. Ind. Appl.*, vol. 59, no. 2, pp. 1944–1955, Mar./Apr. 2023.

[21] J. Zhang, Z. Sun, Q. Zhao, and H. Li, *IEEE Access*, vol. 12, pp. 191120–191128, 2024.

[22] F. Xu, M. Zhu, and Y. Ye, "The stability of LCL-type grid-tied inverter based on repetitive control and grid voltage feed-forward," *IEEE Trans. Emerg. Sel. Topics Power Electron.*, vol. 11, no. 2, pp. 1496–1506, Apr. 2023.

[23] D. G. Holmes and T. A. Lipo, *Pulse Width Modulation for Power Converters: Principles and Practice*. Hoboken, NJ, USA: Wiley, 2003.

[24] T.-L. Tai and J.-S. Chen, "UPS inverter design using discrete-time sliding-mode control scheme," *IEEE Trans. Ind. Electron.*, vol. 49, no. 1, pp. 67–75, Feb. 2002.

[25] X. Hao, X. Yang, T. Liu, L. Huang, and W. Chen, "A sliding-mode controller with multiresonant sliding surface for single-phase grid-connected VSI with an LCL filter," *IEEE Trans. Power Electron.*, vol. 28, no. 5, pp. 2259–2268, May 2013.

[26] R. P. Vieira, L. T. Martins, J. R. Massing, and M. Stefanello, "Sliding mode controller in a multiloop framework for a grid-connected VSI with LCL filter," *IEEE Trans. Ind. Electron.*, vol. 65, no. 6, pp. 4714–4723, Jun. 2018.

[27] N. Altin, S. Ozdemir, H. Komurcugil, I. Sefa, and S. Biricik, "Sliding-mode and proportional-resonant based control strategy for three-phase two-leg T-type grid-connected inverters with LCL filter," in *Proc. IECON 2018-44th Annu. Conf. IEEE Ind. Electron. Soc.*, 2018, pp. 4492–4497.

[28] H. Valderrama-Blavi, J. Bosque, J. Barrado, M. Munoz, and J. Calvente, "Design of a sinusoidal current source using a sliding-mode-controlled asymmetrical full-bridge multilevel converter," *IET Power Electron.*, vol. 1, no. 2, pp. 203–213, 2008.

**Víctor Repecho** received the B.S, M.S., and Ph.D. degrees in electronic engineering from the Universitat Politècnica de Catalunya (UPC), Barcelona, Spain, in 2006, 2012, and 2018, respectively.

Since 2010, he has been a Development Engineer with the Institute of Industrial and Control Engineering, UPC, where, since 2019, he has been an Assistant Professor with the Automatic control Department. His research interests include digital control, nonlinear control, and control of power electronic converters.

**Abel Borràs** was born in Sant Fruitós de Bages, Spain. He received the B.S. degree in electronic engineering from from Universitat Politècnica de Catalunya (UPC), Barcelona, Spain in 2016.

Currently he is working as Applications Engineer with Monolithic Power Systems. His research interests include related to power electronics, energy management, and wide-bandgap power devices.

**Domingo Biel** received the B.S, M.S., and Ph.D. degrees in telecommunications engineering from the Universitat Politècnica de Catalunya (UPC), Barcelona, Spain, in 1990, 1994 and 1999, respectively.

Since 1998, he has been an Associate Professor with the Electronic Engineering Department, UPC, where he teaches power electronics and control theory. His research focuses on nonlinear control and its application to renewable energy systems and power electronics.